

**Numerical solution of partial  
differential equations  
with Powell-Sabin splines**

*Hendrik Speleers*

*Paul Dierckx*

*Stefan Vandewalle*

*Report TW 408, October 2004*



**Katholieke Universiteit Leuven**  
Department of Computer Science  
Celestijnenlaan 200A – B-3001 Heverlee (Belgium)

# Numerical solution of partial differential equations with Powell-Sabin splines

*Hendrik Speleers*

*Paul Dierckx*

*Stefan Vandewalle*

*Report TW 408, October 2004*

Department of Computer Science, K.U.Leuven

## **Abstract**

Powell-Sabin splines are piecewise quadratic polynomials with global  $C^1$ -continuity. They are defined on conformal triangulations of two-dimensional domains, and admit a compact representation in a normalized B-spline basis. Recently, these splines have been used successfully in the area of computer-aided geometric design for the modelling and fitting of surfaces. In this paper, we discuss the applicability of Powell-Sabin splines for the numerical solution of partial differential equations defined on irregular domains. A Galerkin-type PDE discretisation is derived, and elaborated for the variable coefficient diffusion equation. Special emphasis goes to the treatment of Dirichlet and Neumann boundary conditions. Finally, an error estimator is developed and an adaptive mesh refinement strategy is proposed. We will illustrate the effectiveness of the approach by means of some numerical experiments.

**Keywords :** partial differential equations, splines, finite elements, adaptive refinement

**AMS(MOS) Classification :** Primary : 65N30, Secondary : 41A15, 65D07

# Numerical solution of partial differential equations with Powell-Sabin splines

Hendrik Speleers, Paul Dierckx and Stefan Vandewalle

*Department of Computer Science, Katholieke Universiteit Leuven  
Celestijnenlaan 200A, B-3001 Leuven, Belgium*

## Abstract

Powell-Sabin splines are piecewise quadratic polynomials with global  $C^1$ -continuity. They are defined on conformal triangulations of two-dimensional domains, and admit a compact representation in a normalized B-spline basis. Recently, these splines have been used successfully in the area of computer-aided geometric design for the modelling and fitting of surfaces. In this paper, we discuss the applicability of Powell-Sabin splines for the numerical solution of partial differential equations defined on irregular domains. A Galerkin-type PDE discretisation is derived, and elaborated for the variable coefficient diffusion equation. Special emphasis goes to the treatment of Dirichlet and Neumann boundary conditions. Finally, an error estimator is developed and an adaptive mesh refinement strategy is proposed. We will illustrate the effectiveness of the approach by means of some numerical experiments.

*Keywords:* partial differential equations, splines, finite elements, adaptive refinement  
*AMS classification:* 41A15, 65D07, 65N30

## 1 Introduction

The finite element method is a powerful tool for solving partial differential equations (PDEs) numerically. By using a suitable projection, the method determines an approximation to the PDE solution in a carefully selected subset of the solution space. The choice of the approximation space is very important, as it directly affects the accuracy and computational efficiency. In this paper, we consider the use of spline functions as a basis for the PDE solution.

Spline functions are piecewise polynomial functions satisfying certain global smoothness properties. For two-dimensional applications, like surface modelling and fitting, the tensor product splines are today the most commonly used splines, because of their compact representation, their flexibility, ease of implementation and efficiency. A definite drawback, however, is that they are restricted to regular rectangular meshes. Especially in applications with local difficulties, this badly affects the global quality of the approximation, and results in a too high spline dimension.

An alternative is to define piecewise polynomials on irregular triangulations. A triangulation can be locally adapted more easily, and it is also more suited to approximate domains with irregular boundaries. Commonly used piecewise polynomial functions on triangulations [2] are the Lagrange and Hermite piecewise polynomials, with global  $C^0$ -continuity. At the cost of a much larger dimension, the Argyris space of piecewise polynomials on triangles attains global  $C^1$ -continuity. The Powell-Sabin splines considered in this paper constitute a fair compromise. These bivariate quadratic splines on triangulations are  $C^1$ -continuous, and they can be efficiently represented in a compact normalized B-spline basis. These properties ensure that Powell-Sabin B-splines are appropriate candidates for basis functions in finite element applications.

Powell and Sabin [9] studied the use of piecewise quadratic  $C^1$ -continuous polynomials of two variables on triangulations for drawing contour lines of bivariate functions. In that context, they developed a particular triangulation split that led to the so-called Powell-Sabin (PS-)splines. Willemans [15] used these splines for smoothing scattered data. Their application in the area of computer-aided geometric design was considered in [16] by Windmolders. A multiresolution analysis leading to a definition of Powell-Sabin spline wavelets was developed by Vanraes *et al.* in [14] and Windmolders *et al.* in [17]. Here we consider the use of Powell-Sabin splines for solving partial differential equations. We solve the variable coefficient diffusion equation with a Galerkin finite element method, and derive an analytical formulation for the stiffness matrix elements for the case where the diffusion is a constant in each element. We show that the error is of the order  $\mathcal{O}(h_{\max}^3)$ , where  $h_{\max}$  is the longest side of the triangulation. We investigate how to impose certain boundary conditions on the Powell-Sabin spline, and derive the constraints imposed by these conditions on the spline coefficients. A particular choice of the boundary basis splines is suggested that greatly simplifies these constraints. In addition, we develop an a posteriori error estimator, and integrate it in an adaptive mesh refinement strategy.

The paper is organized as follows. Section 2 reviews some general concepts of polynomials on triangulations, and recalls the definition of the Powell-Sabin spline space. That section also covers the relevant aspects of the construction of a normalized B-spline basis and its Bernstein-Bézier representation. In section 3 we treat Dirichlet and Neumann boundary conditions, and consider how we can simplify the constraints imposed by these boundary conditions on the spline coefficients. Section 4 is devoted to the analysis of a Galerkin-type PDE discretisation using PS-splines for a variable coefficient diffusion equation. Finally, in section 5 we end with some concluding remarks.

## 2 Powell-Sabin splines

### 2.1 Bivariate polynomials in the Bernstein-Bézier representation

Consider a non-degenerate triangle  $\rho(V_1, V_2, V_3)$ , defined by vertices  $V_i$  with Cartesian coordinates  $(x_i, y_i) \in \mathbb{R}^2$ ,  $i = 1, 2, 3$ . Any point  $(x, y) \in \mathbb{R}^2$  can be expressed in terms of its barycentric coordinates  $\tau = (\tau_1, \tau_2, \tau_3)$  with respect to  $\rho$ . Let  $\Pi_m$  denote the linear space of bivariate polynomials of total degree less than or equal to  $m$ . Any polynomial  $p_m(x, y) \in \Pi_m$  on the triangle  $\rho$  has a unique representation of the form

$$p_m(x, y) = b_\rho^m(\tau) = \sum_{|\lambda|=m} b_\lambda B_\lambda^m(\tau). \quad (1)$$

Here,  $\lambda = (\lambda_1, \lambda_2, \lambda_3)$  is a multi-index of length  $|\lambda| = \lambda_1 + \lambda_2 + \lambda_3$ , and

$$B_\lambda^m(\tau) = \frac{m!}{\lambda_1! \lambda_2! \lambda_3!} \tau_1^{\lambda_1} \tau_2^{\lambda_2} \tau_3^{\lambda_3} \quad (2)$$

a Bernstein-Bézier polynomial on the triangle [7]. The coefficients  $b_\lambda$  are called the Bézier ordinates of  $p_m(x, y)$ . By associating each ordinate  $b_\lambda$  with the point  $(\frac{\lambda_1}{m}, \frac{\lambda_2}{m}, \frac{\lambda_3}{m})$  in the triangle, we can display this Bernstein-Bézier representation schematically as in Figure 1.

### 2.2 The space of Powell-Sabin splines

Consider a simply connected subset  $\Omega \in \mathbb{R}^2$  with polygonal boundary  $\partial\Omega$ . Assume a conforming triangulation  $\Delta$  of  $\Omega$  is given, consisting of  $t$  triangles  $\rho_j$ ,  $j = 1, \dots, t$ , and having vertices  $V_k$  with Cartesian coordinates  $(x_k, y_k)$ ,  $k = 1, \dots, n$ . The Powell-Sabin (PS-)refinement  $\Delta^*$  of  $\Delta$  partitions each triangle  $\rho_j$  into six smaller triangles with a common vertex  $Z_j$ . This partition is defined algorithmically as follows:

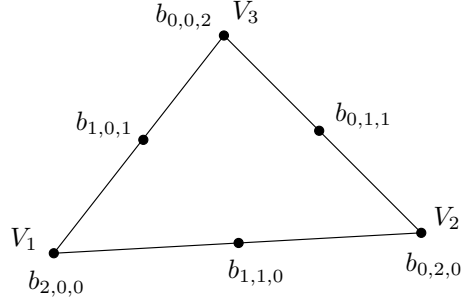


Figure 1: Schematic representation of a quadratic bivariate polynomial by means of its Bézier ordinates  $b_\lambda$  with  $\lambda = (\lambda_1, \lambda_2, \lambda_3)$  and  $|\lambda| = 2$ .

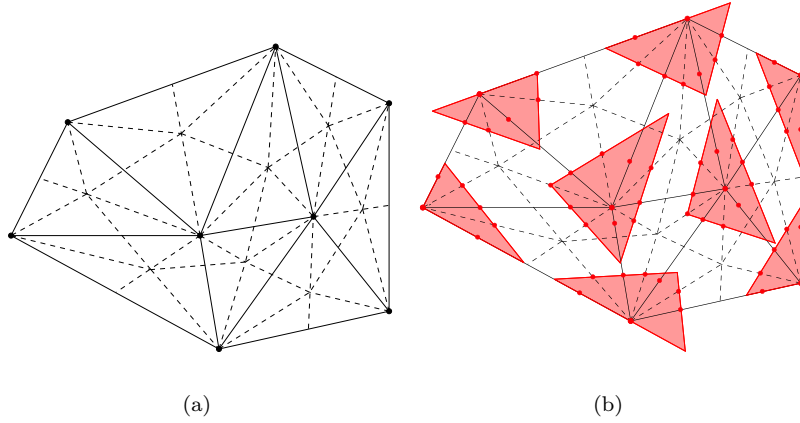


Figure 2: (a) A PS-refinement  $\Delta^*$  (dashed lines) of a given triangulation  $\Delta$  (solid lines); (b) the PS-points (bullets) and a set of suitable PS-triangles (shaded).

1. Choose an interior point  $Z_j$  in each triangle  $\rho_j$ , so that if two triangles  $\rho_i$  and  $\rho_j$  have a common edge, then the line joining  $Z_i$  and  $Z_j$  intersects the common edge at a point  $R_{i,j}$ .
2. Join each point  $Z_j$  to the vertices of  $\rho_j$ .
3. For each edge of the triangle  $\rho_j$ 
  - (a) which belongs to the boundary  $\partial\Omega$ : join  $Z_j$  to an arbitrary point on that edge;
  - (b) which is common to a triangle  $\rho_i$ : join  $Z_j$  to  $R_{i,j}$ .

Figure 2(a) displays a triangulation with 8 elements, and a corresponding PS-refinement containing 48 triangles. The space of piecewise quadratic polynomials on  $\Delta^*$  with global  $C^1$ -continuity is called the Powell-Sabin spline space:

$$S_2^1(\Delta^*) = \left\{ s \in C^1(\Omega) : s|_{\rho_j^*} \in \Pi_2, \rho_j^* \in \Delta^* \right\} \quad (3)$$

Each of the  $6t$  triangles resulting from the PS-refinement is the domain triangle of a quadratic Bernstein-Bézier polynomial, i.e., with  $m = 2$  in equations (1) and (2). Powell and Sabin [9]

proved that the following interpolation problem

$$s(V_l) = f_l, \quad \frac{\partial s}{\partial x}(V_l) = f_{x,l}, \quad \frac{\partial s}{\partial y}(V_l) = f_{y,l}, \quad l = 1, \dots, n. \quad (4)$$

has a unique solution  $s(x, y) \in S_2^1(\Delta^*)$  for any given set of  $n$   $(f_l, f_{x,l}, f_{y,l})$ -values. It follows that the dimension of the Powell-Sabin spline space  $S_2^1(\Delta^*)$  equals  $3n$ .

### 2.3 A normalized B-spline representation

Several authors [6, 11] have considered the construction of a locally supported basis for  $S_2^1(\Delta^*)$ . The general idea is to associate with each vertex  $V_i$  three linearly independent triplets  $(\alpha_{i,j}, \beta_{i,j}, \gamma_{i,j})$ ,  $j = 1, 2, 3$ . The B-spline  $B_i^j(x, y)$  can be found as the unique solution of interpolation problem (4) with all  $(f_l, f_{x,l}, f_{y,l}) = (0, 0, 0)$  except for  $l = i$ , where  $(f_i, f_{x,i}, f_{y,i}) = (\alpha_{i,j}, \beta_{i,j}, \gamma_{i,j}) \neq (0, 0, 0)$ . It is easy to see that this B-spline has a local support:  $B_i^j(x, y)$  vanishes outside the union of all triangles containing  $V_i$ . Every Powell-Sabin spline can then be represented as

$$s(x, y) = \sum_{i=1}^n \sum_{j=1}^3 c_{i,j} B_i^j(x, y). \quad (5)$$

The basis forms a convex partition of unity on  $\Omega$  if

$$B_i^j(x, y) \geq 0, \quad \text{and} \quad \sum_{i=1}^n \sum_{j=1}^3 B_i^j(x, y) = 1, \quad (6)$$

for all  $(x, y) \in \Omega$ . This property, together with the local support of the Powell-Sabin B-splines, lies at the basis of their computational effectiveness for computer-aided geometric design applications.

In [5] Dierckx has presented a geometrical way to derive and construct such a normalized basis:

1. For each vertex  $V_i \in \Delta$ , identify the corresponding PS-points. These are defined as the midpoints of all edges in the PS-refinement  $\Delta^*$  containing  $V_i$ . The vertex  $V_i$  itself is also a PS-point. In Figure 2(b) the PS-points are indicated as bullets.
2. For each vertex  $V_i$ , find a triangle  $t_i(Q_{i,1}, Q_{i,2}, Q_{i,3})$  containing all the PS-points of  $V_i$ . Denote its vertices  $Q_{i,j}(X_{i,j}, Y_{i,j})$ . The triangles  $t_i$ ,  $i = 1, \dots, n$  are called PS-triangles. Note that the PS-triangles are not uniquely defined. Figure 2(b) shows some PS-triangles. One possibility for their construction [5] is to calculate a triangle of minimal area. Computationally, this problem leads to a quadratic programming problem. An alternative solution is given in [13], where the sides of the PS-triangle are found by connecting two PS-points.
3. The three linearly independent triplets  $(\alpha_{i,j}, \beta_{i,j}, \gamma_{i,j})$ ,  $j = 1, 2, 3$  are derived from the PS-triangle  $t_i$  of a vertex  $V_i$  as follows:

$$\alpha_i = (\alpha_{i,1}, \alpha_{i,2}, \alpha_{i,3}) \text{ are the barycentric coordinates of } V_i \text{ with respect to } t_i, \quad (7a)$$

$$\beta_i = (\beta_{i,1}, \beta_{i,2}, \beta_{i,3}) = (Y_{i,2} - Y_{i,3}, Y_{i,3} - Y_{i,1}, Y_{i,1} - Y_{i,2})/E, \quad (7b)$$

$$\gamma_i = (\gamma_{i,1}, \gamma_{i,2}, \gamma_{i,3}) = (X_{i,3} - X_{i,2}, X_{i,1} - X_{i,3}, X_{i,2} - X_{i,1})/E, \quad (7c)$$

$$\text{where } E = \begin{vmatrix} X_{i,1} & Y_{i,1} & 1 \\ X_{i,2} & Y_{i,2} & 1 \\ X_{i,3} & Y_{i,3} & 1 \end{vmatrix}.$$

Note that  $|\alpha_i| = 1$  and  $|\beta_i| = |\gamma_i| = 0$ . The fact that the PS-triangle  $t_i$  contains the PS-points of the vertex  $V_i$  guarantees the positivity property of (6).

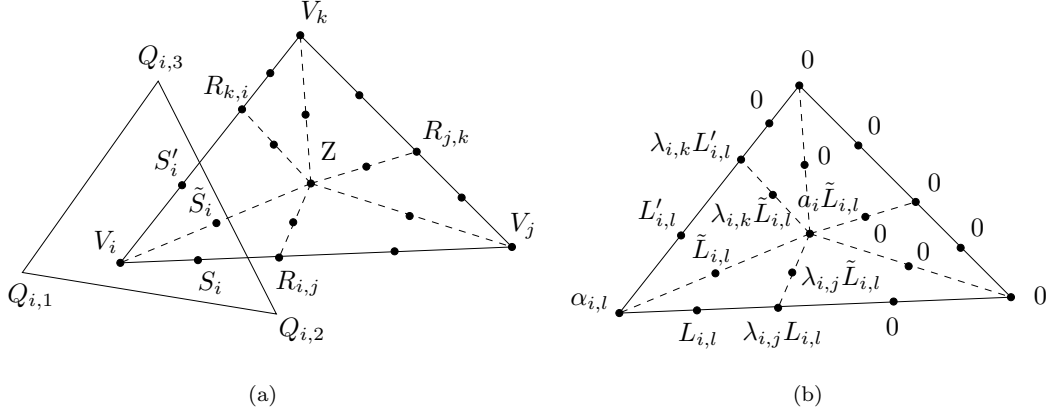


Figure 3: (a) PS-refinement of triangle  $\rho(V_i, V_j, V_k)$  together with PS-triangle  $t_i(Q_{i,1}, Q_{i,2}, Q_{i,3})$  of vertex  $V_i$ ; (b) schematic representation of the Bézier ordinates of a Powell-Sabin B-spline  $B_i^l(x, y)$ .

## 2.4 The Bernstein-Bézier representation of a Powell-Sabin B-spline

Consider a domain triangle  $\rho(V_i, V_j, V_k) \in \Delta$  with its PS-refinement  $\Delta^*$ , as in Figure 3(a). The points indicated in the Figure have the following barycentric coordinates:  $V_i(1, 0, 0)$ ,  $V_j(0, 1, 0)$ ,  $V_k(0, 0, 1)$ ,  $Z(a_i, a_j, a_k)$ ,  $R_{i,j}(\lambda_{i,j}, \lambda_{j,i}, 0)$ ,  $R_{j,k}(0, \lambda_{j,k}, \lambda_{k,j})$ , and  $R_{k,i}(\lambda_{k,i}, 0, \lambda_{i,k})$ . On each of the six triangles in  $\Delta^*$  the B-spline is a quadratic polynomial, that can be represented in its Bernstein-Bézier formulation by means of Bézier ordinates. In [6] the values of the Bézier ordinates of the basis function  $B_i^l(x, y)$  corresponding to the triplet  $(\alpha_{i,l}, \beta_{i,l}, \gamma_{i,l})$  are derived. The outcome is schematically represented in Figure 3(b), with

$$L_{i,l} = \alpha_{i,l} + \frac{\lambda_{j,i}}{2} \bar{\beta}, \quad L'_{i,l} = \alpha_{i,l} + \frac{\lambda_{k,i}}{2} \bar{\gamma}, \quad \tilde{L}_{i,l} = \alpha_{i,l} + \frac{a_j}{2} \bar{\beta} + \frac{a_k}{2} \bar{\gamma}, \quad (8)$$

and

$$\bar{\beta} = \beta_{i,l}(x_j - x_i) + \gamma_{i,l}(y_j - y_i), \quad \bar{\gamma} = \beta_{i,l}(x_k - x_i) + \gamma_{i,l}(y_k - y_i). \quad (9)$$

As was shown in [6], the values  $(\alpha_{i,1}, \alpha_{i,2}, \alpha_{i,3})$ ,  $(L_{i,1}, L_{i,2}, L_{i,3})$ ,  $(L'_{i,1}, L'_{i,2}, L'_{i,3})$  and  $(\tilde{L}_{i,1}, \tilde{L}_{i,2}, \tilde{L}_{i,3})$  of the three basis splines associated with  $V_i$  are the barycentric coordinates of the PS-points  $V_i$ ,  $S_i$ ,  $S'_i$ , and  $\tilde{S}_i$  with respect to the PS-triangle  $t_i(Q_{i,1}, Q_{i,2}, Q_{i,3})$ .

In this Bernstein-Bézier representation the B-splines can easily be manipulated. Using the de Casteljau algorithm [7] evaluation and differentiation is possible in a numerically stable way. The integral of a Powell-Sabin B-spline on a subtriangle  $\rho^* \in \Delta^*$  is reduced to a weighted sum of its Bézier ordinates [1]:

$$\int_{\rho^*} B_i^j(x, y) dx dy = \frac{A(\rho^*)}{6} \sum_{|\lambda|=2} b_\lambda, \quad (10)$$

with  $A(\rho^*)$  the area of  $\rho^*$ .

## 3 Powell-Sabin splines with specified boundary conditions

We address the question of how to impose certain boundary conditions on a Powell-Sabin spline. First we consider the case of a specified boundary value, i.e., the Dirichlet boundary condition. In §3.2 we explain how to impose a specified normal derivative, or Neumann boundary condition.

### 3.1 A Dirichlet boundary condition

When solving a PDE with Powell-Sabin splines, one will often be faced with the following question:

$$\text{find a } s(x, y) \in S_2^1(\Delta^*) \text{ such that } s(x, y) = f(x, y) \text{ for all } (x, y) \in \partial\Omega. \quad (11)$$

Usually, a Powell-Sabin spline cannot exactly satisfy this boundary condition for arbitrary  $f(x, y)$ . Indeed, by the nature of the PS-spline, its trace along the boundary is a one-dimensional piecewise quadratic polynomial with certain continuity characteristics. It is  $C^1$ -continuous at the interior points  $R_{i,j}$  of the boundary sides; it is typically  $C^0$ -continuous at the boundary vertices  $V_i$  if the adjacent triangle sides intersect at an angle different from  $\pi$ , and  $C^1$ -continuous at  $V_i$  otherwise. Further on, we will assume that the function  $f(x, y)$  is consistent with the PS-spline continuity characteristics. Let  $w$  denote the accumulated arc length along  $\partial\Omega$ , and let  $\tilde{s}(w)$  and  $\tilde{f}(w)$  denote the corresponding functions  $s(x, y)$  and  $f(x, y)$  on this boundary. It will turn out convenient to describe  $\tilde{s}(w)$  as a one-dimensional generalized (periodic) quadratic spline in the classical B-spline representation [3]. Single knots, denoted as  $t_{i,j}$ , are then associated with the points  $R_{i,j}$ ; double knots, denoted as  $t_{i_1}$  and  $t_{i_2}$ , are assigned to the edge points  $V_i$  in the case of an edge intersection different from  $\pi$ . A single knot  $t_{i_1}$  will be used in the case of an angle  $\pi$  intersection. The lengths of the knot intervals are chosen so as to preserve the distances between the points  $R_{i,j}$  and  $V_i$ . The notation and knot positions are illustrated in Figure 4(a).

A quadratic B-spline refers to four successive knots and the support of the B-spline is the interval spanned by these knots. Let  $N_k(w)$  be the B-splines with  $t_k$  as first knot, we can consider the representation

$$\tilde{s}(w) = \sum_k b_k N_k(w). \quad (12)$$

In a preprocessing step we can easily determine the coefficients  $b_k$  by a least squares algorithm given an appropriate set of  $(w_l, \tilde{f}(w_l))$ -values [4]. Once the coefficients are known, we wish to formulate the constraints on the coefficients  $c_{i,j}$  in (5) such that (11) is satisfied (approximately). For each vertex  $V_j$  on the boundary, with an edge intersection angle different from  $\pi$ , we impose the three conditions

$$s(V_j) = \tilde{s}(t_{j_1}), \quad \frac{\partial}{\partial t_l} s(V_j) = \tilde{s}'(t_{j_1} -), \quad \text{and} \quad \frac{\partial}{\partial t_r} s(V_j) = \tilde{s}'(t_{j_1} +). \quad (13)$$

Here,  $\frac{\partial}{\partial t_l}$  and  $\frac{\partial}{\partial t_r}$  denote the tangential derivative along  $\partial\Omega$  in clockwise and in counter-clockwise respectively. In the case the intersection angle equals  $\pi$ , the conditions are

$$s(V_j) = \tilde{s}(t_{j_1}), \quad \text{and} \quad \frac{\partial}{\partial t} s(V_j) = \tilde{s}'(t_{j_1}), \quad (14)$$

with  $\frac{\partial}{\partial t}$  being the tangential derivative.

With the interpolation conditions (4), the definition of the triplets  $(\alpha_{j,m}, \beta_{j,m}, \gamma_{j,m})$ , and using the properties of one-dimensionale B-splines, one finds that (13) is equivalent to the three constraints

$$\sum_{m=1}^3 c_{j,m} \alpha_{j,m} = b_{i,j}, \quad (15a)$$

$$\sum_{m=1}^3 c_{j,m} [(x_i - x_j) \beta_{j,m} + (y_i - y_j) \gamma_{j,m}] = \frac{2}{\lambda_{i,j}} (b_{i_2} - b_{i,j}), \quad (15b)$$

$$\sum_{m=1}^3 c_{j,m} [(x_k - x_j) \beta_{j,m} + (y_k - y_j) \gamma_{j,m}] = \frac{2}{\lambda_{k,j}} (b_{j_1} - b_{i,j}). \quad (15c)$$

These general constraints can be simplified considerably by a careful selection of the PS-triangle associated with  $V_j$ . We choose the sides of this PS-triangle parallel to the boundary,

$$Q_{j,1} = V_j, \quad Q_{j,2} = V_j + \delta_{i,j}(V_i - V_j), \quad \text{and} \quad Q_{j,3} = V_j + \delta_{k,j}(V_k - V_j), \quad (16)$$

with the values  $\delta_{i,j}$  and  $\delta_{k,j}$  such that this triangle contains all the PS-points of vertex  $V_j$ , see the left panel of Figure 4(b). Then, the constraints (15) simplify to

$$c_{j,1} = b_{i,j}, \quad (17a)$$

$$c_{j,2} = b_{i,j} + \frac{2\delta_{i,j}}{\lambda_{i,j}}(b_{i_2} - b_{i,j}), \quad (17b)$$

$$c_{j,3} = b_{i,j} + \frac{2\delta_{k,j}}{\lambda_{k,j}}(b_{j_1} - b_{i,j}). \quad (17c)$$

Notice that a homogeneous Dirichlet boundary condition requires all coefficients  $c_{j,m}$  to be zero.

If the boundary forms a straight angle at vertex  $V_j$ , constraints (14) become

$$\sum_{m=1}^3 c_{j,m} \alpha_{j,m} = \delta b_{i,j} + (1 - \delta) b_{i_2}, \quad \text{with } \delta = \frac{|t_{j_1} - t_{i,j}|}{|t_{j,k} - t_{i,j}|}, \quad (18a)$$

$$\sum_{m=1}^3 c_{j,m} [(x_i - x_j) \beta_{j,m} + (y_i - y_j) \gamma_{j,m}] = \frac{2\delta}{\lambda_{i,j}} (b_{i_2} - b_{i,j}). \quad (18b)$$

In that situation it is advantageous to use a PS-triangle with one side parallel to the boundary, as depicted in the right panel of Figure 4(b). Let

$$\|Q_{j,1} - Q_{j,2}\| = \delta_{i,j} \|V_i - V_j\|, \quad (19)$$

then the constraints (18) simplify to

$$c_{j,1} = b_{i_2} + \delta \left( 1 - \frac{2\delta_{i,j}}{\lambda_{i,j}} \alpha_{j,2} \right) (b_{i,j} - b_{i_2}), \quad (20a)$$

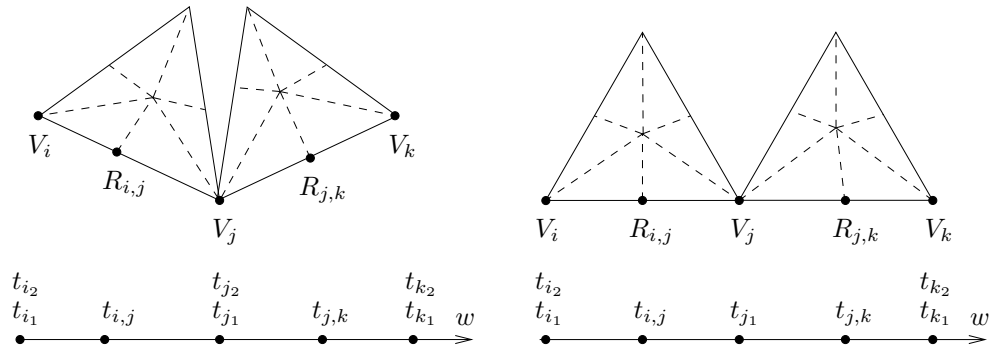
$$c_{j,2} = b_{i_2} + \delta \left( 1 + \frac{2\delta_{i,j}}{\lambda_{i,j}} \alpha_{j,1} \right) (b_{i,j} - b_{i_2}). \quad (20b)$$

With this choice of PS-triangle the Powell-Sabin B-spline  $B_j^3$  vanishes at the boundary. The value of the corresponding coefficient  $c_{j,3}$  is not constrained by the Dirichlet boundary condition.

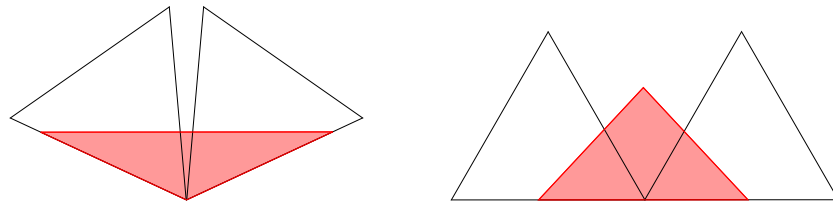
Note that the linear system (15) for the coefficient  $c_{j,m}$  becomes increasingly ill-conditioned when the intersection angle approaches the value  $\pi$ . In that case, equations (15b)-(15c) become closer and closer to being linearly dependent. This is reflected into a PS-triangle that becomes increasingly large, and leads to a poorly conditioned PS B-spline basis. More precisely, consider the determinant of the system (15) for the unknowns  $c_{j,m}$ :

$$\begin{aligned} & \begin{vmatrix} \alpha_{j,1} & \alpha_{j,2} & \alpha_{j,3} \\ (x_i - x_j)\beta_{j,1} + (y_i - y_j)\gamma_{j,1} & (x_i - x_j)\beta_{j,2} + (y_i - y_j)\gamma_{j,2} & (x_i - x_j)\beta_{j,3} + (y_i - y_j)\gamma_{j,3} \\ (x_k - x_j)\beta_{j,1} + (y_k - y_j)\gamma_{j,1} & (x_k - x_j)\beta_{j,2} + (y_k - y_j)\gamma_{j,2} & (x_k - x_j)\beta_{j,3} + (y_k - y_j)\gamma_{j,3} \end{vmatrix} \\ &= \begin{vmatrix} 1 & x_j & y_j \\ 1 & x_i & y_j \\ 1 & x_k & y_j \end{vmatrix} \begin{vmatrix} \alpha_{j,1} & \alpha_{j,2} & \alpha_{j,3} \\ \beta_{j,1} & \beta_{j,2} & \beta_{j,3} \\ \gamma_{j,1} & \gamma_{j,2} & \gamma_{j,3} \end{vmatrix} = \frac{A(\rho(V_i, V_j, V_k))}{A(t_j(Q_{j,1}, Q_{j,2}, Q_{j,3}))} = \frac{1}{\delta_{i,j} \delta_{k,j}}. \end{aligned} \quad (21)$$

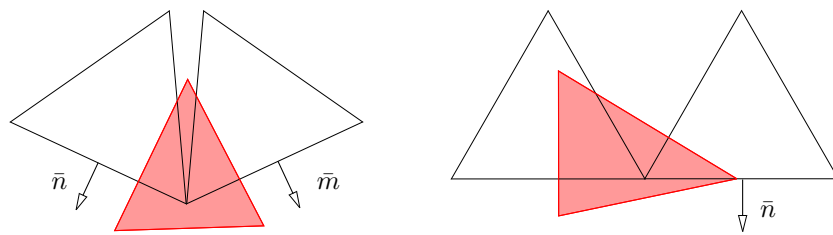
Hence, this determinant vanishes when the angle approaches  $\pi$ . For an angle sufficiently close to  $\pi$ , we therefore propose to impose conditions (14) rather than (13), e.g., as soon as  $\delta_{i,j} \delta_{k,j} > 100$ , and to use constraints (20) with a PS-triangle subject to (19).



(a) Knot positions



(b) Dirichlet boundary



(c) Neumann boundary

Figure 4: (a) The position of the B-spline knots for the representation of a quadratic boundary spline; (b)-(c) a choice of PS-triangles that leads to an easier formulation of boundary conditions.

### 3.2 Neumann boundary condition

In a Galerkin approach, a Neumann condition does not strictly need to be enforced on the elements of the solution space. As natural boundary conditions, they are usually satisfied automatically. We will nevertheless consider how to impose a normal derivative on a PS-spline, as it is certainly useful in, e.g., collocation methods for PDEs. We will treat Neumann conditions with a similar line of arguments as we did for Dirichlet conditions in §3.1. Here, we deal with the question

$$\text{find a } s(x, y) \in S_2^1(\Delta^*) \text{ such that } \frac{\partial}{\partial \bar{n}} s(x, y) = f(x, y) \text{ for all } (x, y) \in \partial\Omega, \quad (22)$$

where  $\frac{\partial}{\partial \bar{n}}$  denotes the outward normal derivative. We note that the outward normal is constant on each boundary side. We will assume that the function  $f(x, y)$  satisfies the continuity behaviour of the considered piecewise linear derivative function of the PS-spline. It is  $C^0$ -continuous at the points  $R_{i,j}$  if the interior side  $R_{i,j}$ - $Z_{i,j,l}$  is not parallel to  $\bar{n}$ , and  $C^1$ -continuous at  $R_{i,j}$  otherwise. It is discontinuous at the boundary vertices  $V_i$  if the adjacent triangle sides intersect at an angle different from  $\pi$ , and  $C^0$ -continuous at  $V_i$  otherwise. Let  $w$  denote the accumulated arc length along  $\partial\Omega$ , and  $\hat{s}(w)$  the corresponding function  $\frac{\partial}{\partial \bar{n}} s(x, y)$  on this boundary. We will describe  $\hat{s}(w)$  by a one-dimensional generalized (periodic) linear spline in a B-spline representation with the knot positions shown in Figure 4(a). The linear B-splines are defined on an interval spanned by three knots. The corresponding coefficients  $b_k$  can be determined by a least squares algorithm as in §3.1.

On each boundary side  $V_i$ - $V_j$  of a triangle  $\rho(V_i, V_j, V_l)$  we impose the three conditions

$$\frac{\partial}{\partial \bar{n}} s(V_i) = \hat{s}(t_{i_1}), \quad \frac{\partial}{\partial \bar{n}} s(V_j) = \hat{s}(t_{j_1}), \quad \text{and} \quad \frac{\partial}{\partial \bar{n}} s(R_{i,j}) = \hat{s}(t_{i,j}). \quad (23)$$

In order to simplify further algebraic manipulation, it turned out that it is advantageous to replace the last equation by the equivalent formula

$$\frac{\partial}{\partial \bar{n}} s(R_{i,j}) - \lambda_{i,j} \frac{\partial}{\partial \bar{n}} s(V_i) - \lambda_{j,i} \frac{\partial}{\partial \bar{n}} s(V_j) = \hat{s}(t_{i,j}) - \lambda_{i,j} \hat{s}(t_{i_1}) - \lambda_{j,i} \hat{s}(t_{j_1}). \quad (24)$$

Using the Bernstein-Bézier representation of §2.4, this leads to the constraints

$$\sum_{m=1}^3 c_{i,m} [\bar{n}_x \beta_{i,m} + \bar{n}_y \gamma_{i,m}] = b_{i,1}, \quad (25a)$$

$$\sum_{m=1}^3 c_{j,m} [\bar{n}_x \beta_{j,m} + \bar{n}_y \gamma_{j,m}] = b_{i,j}, \quad (25b)$$

$$2\epsilon \left( \sum_{m=1}^3 c_{i,m} \left[ \alpha_{i,m} + \frac{\bar{\beta}_{i,m}}{2} \right] - \sum_{m=1}^3 c_{j,m} \left[ \alpha_{j,m} + \frac{\bar{\gamma}_{j,m}}{2} \right] \right) = b_{i_2} - \lambda_{i,j} b_{i_1} - \lambda_{j,i} b_{i,j}, \quad (25c)$$

with

$$\epsilon = \frac{[\bar{n} \times (R_{i,j} - Z_{i,j,l})]_z}{a_l [(V_j - V_i) \times (V_l - V_i)]_z}, \quad (26)$$

where  $[\cdot \times \cdot]_z$  denotes the  $z$ -component of a cross product. The triplets  $(\alpha_{i,m} + \bar{\beta}_{i,m}/2, m = 1, 2, 3)$  and  $(\alpha_{j,m} + \bar{\gamma}_{j,m}/2, m = 1, 2, 3)$  can be interpreted as the barycentric coordinates of the midpoint of the side  $V_i$ - $V_j$  with respect to the PS-triangles  $t_i$  and  $t_j$ . Combining (26) with the formula for the outward normal direction, i.e.,  $\bar{n} = (y_j - y_i, x_i - x_j) / \|V_j - V_i\|$ , we can rewrite  $\epsilon$  as

$$\epsilon = \frac{\cotg \theta}{\|V_j - V_i\|}, \quad (27)$$

where  $\theta$  is the angle between the sides  $Z_{i,j,l}$ - $R_{i,j}$  and  $V_i$ - $V_j$ . If we choose the side  $Q_{i,2}$ - $Q_{i,3}$  of the PS-triangle of vertex  $V_i$  parallel to the direction  $\bar{n}$ , equation (25a) simplifies to

$$(c_{i,2} - c_{i,3})[\bar{n}_x\beta_{i,2} + \bar{n}_y\gamma_{i,2}] = b_{i,1}. \quad (28)$$

Analogously we can simplify equation (25b). Figure 4(c) shows such a PS-triangle.

Finally, we treat two special cases. According to the continuity behaviour of  $\frac{\partial}{\partial \bar{n}}s(V_j)$  at the boundary for an edge intersection angle equal to  $\pi$ , we consider the constraints (25a)-(25c) on the left adjacent boundary side, and only (25b)-(25c) on the right adjacent boundary side. In case of an interior side  $R_{i,j}$ - $Z_{i,j,l}$  parallel to  $\bar{n}$ , we omit equation (25c) because the left hand side is zero. Some caution is again called for angles close to  $\pi$  because the linear system (25) becomes ill-conditioned.

## 4 Galerkin discretisation with Powell-Sabin splines

### 4.1 Model problem

We consider the variable coefficient diffusion equation

$$\nabla \cdot (a\nabla u) + f = 0, \quad \text{in } \Omega \in \mathbb{R}^2 \quad (29)$$

with Dirichlet and Neumann conditions on the boundary segments  $\partial\Omega_D$  and  $\partial\Omega_N$  respectively,

$$u = g_D \text{ on } \partial\Omega_D, \text{ and } \bar{n} \cdot a\nabla u = g_N \text{ on } \partial\Omega_N. \quad (30)$$

Here,  $a$  is assumed to be a positive diagonal matrix, and  $\bar{n}$  is the outward unit normal on the boundary. The variational weak form of (29) is given by

$$\oint_{\partial\Omega_N} v a\nabla u \cdot \bar{n} \, d\Omega - \int_{\Omega} (\nabla v \cdot a\nabla u - vf) \, d\Omega = 0, \quad \forall v \in V \quad (31)$$

where  $V = \{v \in H_0^1(\Omega) : v = 0 \text{ on } \partial\Omega_D\}$ . We will construct a Powell-Sabin spline approximation of the form (5) to the PDE solution  $u$ , and use the standard Galerkin approach for the discretisation of (31). That is, we use the normalized B-spline basis functions as test functions, which lead to a set of linearly independent equations for the unknown Powell-Sabin B-spline coefficients.

### 4.2 The stiffness matrix

The elements of the stiffness matrix are the energy scalar products of two PS B-splines. E.g., with an appropriate ordering of the unknowns, the element on row  $3i + j$  and column  $3k + l$  is given by

$$(B_i^j, B_k^l)_E = \int_{\Omega} \nabla B_i^j \cdot a\nabla B_k^l \, d\Omega. \quad (32)$$

These elements can be computed analytically, if  $a$  is assumed to be constant in each triangle of the PS-refinement. We derive a formula for the integral of the product of derivatives of Bernstein-Bézier polynomials. It can easily be seen that (32) is composed of a sum of such contributions.

With  $D_\alpha b(\tau)$  we denote the directional derivative of the Bernstein-Bézier polynomial  $b(\tau)$  with unit barycentric direction  $\alpha$  on triangle  $\rho$ . Using the de Casteljau algorithm [7], we obtain  $D_\alpha b(\tau) = 2[\tau_1 k_1 + \tau_2 k_2 + \tau_3 k_3]$ , with  $k_1 = \alpha_1 b_{200} + \alpha_2 b_{110} + \alpha_3 b_{101}$ ,  $k_2 = \alpha_1 b_{110} + \alpha_2 b_{020} + \alpha_3 b_{011}$ , and  $k_3 = \alpha_1 b_{101} + \alpha_2 b_{011} + \alpha_3 b_{002}$ . Derivative  $D_\beta d(\tau)$  can be formulated analogously with as coefficients

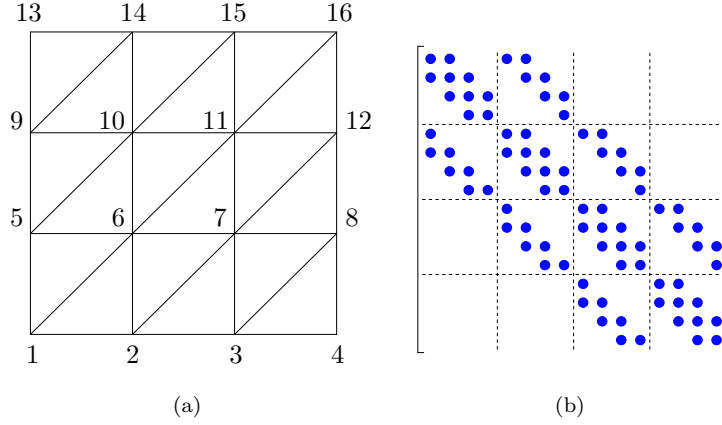


Figure 5: Structure of the stiffness matrix for a regular mesh. Every bullet stands for a non-zero  $3 \times 3$  submatrix.

the values  $l_i$ ,  $i = 1, 2, 3$ . The product of both derivatives is again a quadratic polynomial. Keeping (10) in mind, we obtain that after some technical but elementary computations

$$\int_{\rho} D_{\alpha} b(\tau) D_{\beta} d(\tau) dx dy = \frac{A(\rho)}{3} [(k_1 + k_2 + k_3)(l_1 + l_2 + l_3) + (k_1 l_1 + k_2 l_2 + k_3 l_3)]. \quad (33)$$

Using the unit barycentric directions along the  $x$  and  $y$  direction,

$$\alpha_x = (y_2 - y_3, y_3 - y_1, y_1 - y_2)/F, \quad \alpha_y = (x_3 - x_2, x_1 - x_3, x_2 - x_1)/F, \quad (34)$$

with

$$F = \begin{vmatrix} x_1 & y_1 & 1 \\ x_2 & y_2 & 1 \\ x_3 & y_3 & 1 \end{vmatrix},$$

we can proceed to compose the energy scalar product (32). Since two PS B-splines overlap at most on two adjacent triangles in  $\Delta$ , there will be at most 12 contributions of type (33) to obtain (32).

Because of the local support of the PS B-splines, the stiffness matrix has a sparse structure. Figure 5(b) shows the matrix structure for the regular mesh in Figure 5(a). If there are  $n$  vertices, the matrix has dimension  $3n$ . For this regular mesh, the stiffness matrix can be split into blocks of dimension  $3\sqrt{n}$ . Only the three blocks around the diagonal will contain non-zero elements.

In general, the matrix density, i.e., the number of non-zero elements over the total number of elements, is given by

$$d = \frac{n + 2e}{n^2} < \frac{7}{n}, \quad (35)$$

with  $n$  the number of vertices, and  $e$  the number of edges in the triangulation. There are on average 21 non-zero elements in each row. In comparison with other  $C^1$ -continuous finite elements, the Powell-Sabin stiffness matrix is slightly more dense, but has a much smaller dimension. With Argyris elements, e.g., the matrix dimension is about  $9n$ , three times larger than with PS splines.

### 4.3 Accuracy of the Powell Sabin spline solution

In finite element spaces containing piecewise polynomials of degree  $p$  on triangulations, the error behaves asymptotically as

$$\|u - U\|_{L_2(\Omega)} \leq C h_{\max}^{p+1}, \quad (36)$$

problem	solution $u(x, y)$
1	$\sin(\pi x) \sin(\pi y) + \frac{1}{2} \sin(3\pi x) \sin(2\pi y) + \frac{1}{5} \sin(5\pi x) \sin(8\pi y)$
2	$\frac{(x^2 - x)(y^2 - y)}{0.001 + (x - 0.3)^2 + (y - 0.4)^2}$

Table 1: The solutions of the test problems.

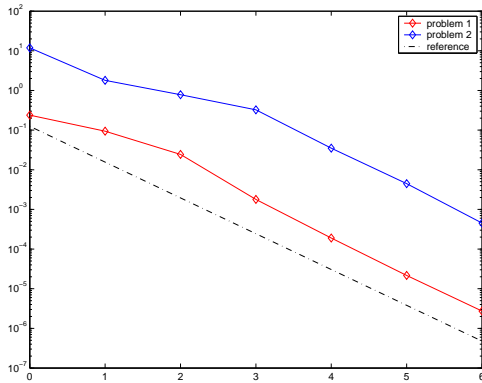
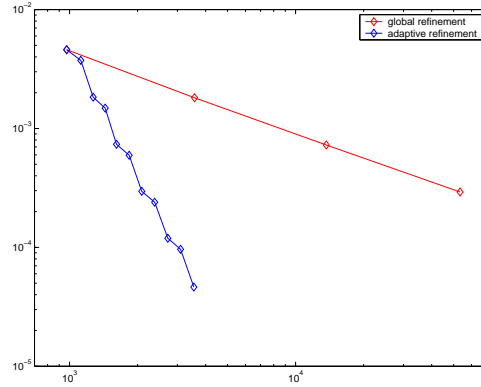
 $L_2$ -norm of error versus number of refinement steps $L_2$ -norm of error versus dimension of system

Figure 6: The  $L_2$ -norm of the error for some test problems on successively refined uniform meshes.

Figure 7: A comparison of the  $L_2$ -norm of the error for global and adaptive refinement on an L-shaped domain.

with  $h_{\max}$  the longest side of the triangulation [12]. Because Powell-Sabin splines are quadratic, in our case the error has order  $\mathcal{O}(h_{\max}^3)$ . We illustrate this convergence rate with some examples.

Suppose a problem of the form (29), with  $a = 1$ , in  $\Omega = [0, 1] \times [0, 1]$ , and  $u = 0$  on  $\partial\Omega$ , where  $f$  is chosen such that the solutions  $u$  correspond to the functions of Table 1. To check the error rate, we will solve each problem on successively refined uniform triangulations, similar to the mesh in Figure 5(a). The initial mesh contains four triangles; the other meshes are obtained by successively halving the mesh size. The Dirichlet boundary conditions are taken into account and explicitly eliminated for the linear system by using equations (17) and (20). Figure 6 shows the reduction of the errors in the  $L_2$ -norm. The dashed line represents the reference function  $h^3$ .

The next considered problem is  $\frac{\partial^2 u}{\partial x^2} + 2\frac{\partial^2 u}{\partial y^2} + 1 = 0$ , defined on the pear-shaped domain shown in Figure 8(a) with a homogeneous Dirichlet boundary condition. Figure 8(b) depicts the  $L_2$ -norm of the error for successively globally refined meshes. The error rate is slightly slower than the reference function  $h_{\max}^3$ .

#### 4.4 An adaptive mesh refinement strategy

An advantage of using finite element methods on triangulations is the ease with which an adaptive mesh refinement can be performed. To that end, we need a cheap and accurate error estimator to locate the triangles with a large error contribution, and a local refinement algorithm to split these triangles.

Using the so-called Aubin-Nitsche trick [8], i.e., by also considering the dual of the model problem,

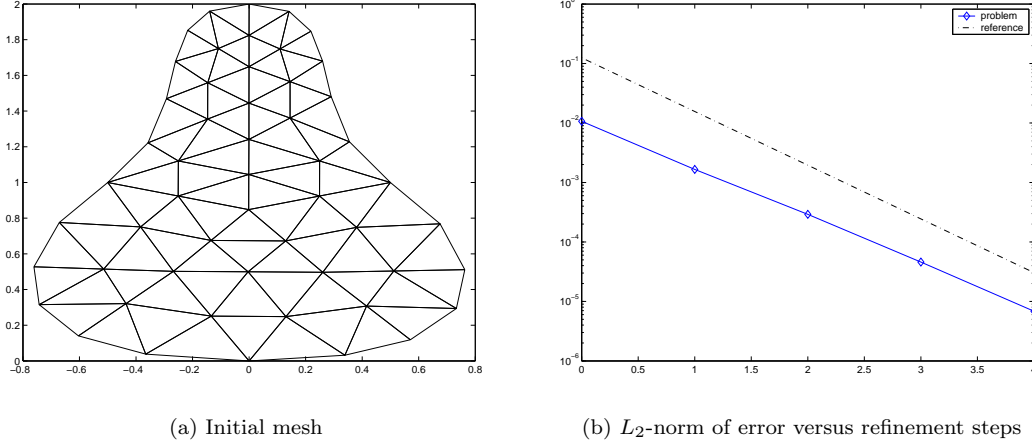


Figure 8: The  $L_2$ -norm of the error for a test problem on successively refined pear-shaped meshes.

an a posteriori  $L_2$ -estimate of the error can easily be derived in the case of PS-splines. We find

$$\|e\|_{L_2} \leq C \left( \sum_{\rho \in \Delta} \frac{h_{\max, \rho}^4}{a_{\min, \rho}^2} \|r\|_{L_2(\rho)}^2 \right)^{1/2}, \quad (37)$$

with  $h_{\max, \rho}$  the longest side of triangle  $\rho$ , with  $a_{\min, \rho}$  the minimum value of the diffusion coefficient on  $\rho$ , and with  $r = \nabla \cdot (a \nabla s) + f$ . An estimate for the local error contribution, is

$$\eta_{L_2, \rho} = \frac{h_{\max, \rho}^2}{a_{\min, \rho}} \|r\|_{L_2(\rho)}. \quad (38)$$

This formula is easy to evaluate on each triangle, and leads to a good indication of the error distribution when the diffusion coefficients are bounded. Based on this error indicator, we can identify elements for refinement. To locally refine the triangulation, we will use an algorithm originally developed by Rivara [10]. The algorithm is graphically illustrated in Figure 9. Suppose we want to refine a triangulation  $\Delta$  by splitting up triangle  $\rho \in \Delta$ , then the Rivara refinement proceeds as follows:

1. Bisect the triangle  $\rho$  by the midpoint  $P$  of the longest side.
2. (*Propagation*) While  $P$  is a non-conforming node of a triangle  $\hat{\rho}$ :
  - (a) bisect  $\hat{\rho}$  by the midpoint  $Q$  of its longest side.
  - (b) if  $P \neq Q$ , join  $P$  to  $Q$ .
  - (c) set  $P = Q$ .

Rivara proved that this algorithm terminates in a finite number of steps, and that it guarantees that no numerically degenerate triangles will be created.

We apply the adaptive mesh refinement strategy to a problem with a geometrical singularity. We consider the L-shaped domain  $\Omega = [0, 1] \times [0, 1] \setminus (0.5, 1] \times (0.4, 1]$ , shown in Figure 10(a), and solve the Poisson equation  $-\nabla^2 u = 1$  in  $\Omega$ , with boundary conditions

$$u = 0 \text{ on } \Gamma_{D_1} = \partial\Omega|_{x=1}, \quad u = 1 \text{ on } \Gamma_{D_2} = \partial\Omega|_{y=1}, \quad \text{and} \quad \frac{\partial u}{\partial \bar{n}} = 0 \text{ on } \Gamma_N = \partial\Omega \setminus (\Gamma_{D_1} \cup \Gamma_{D_2}).$$

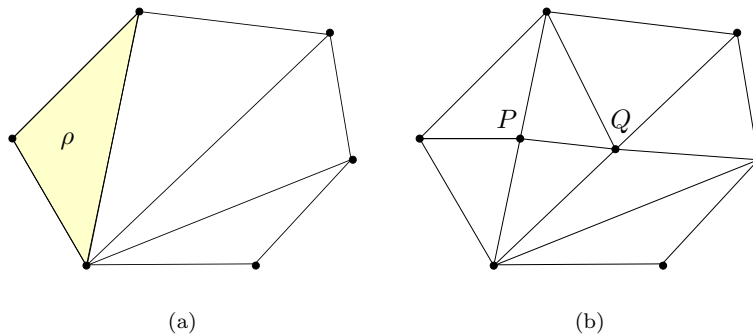
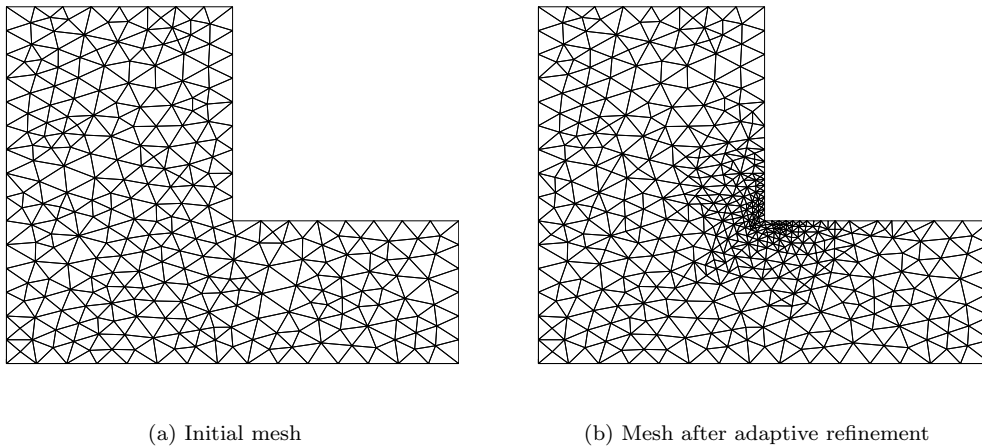
Figure 9: The Rivara algorithm starting with a split of triangle  $\rho$ .

Figure 10: An adaptive refinement on a geometrical singularity.

In an adaptive refinement step we decided to split ten per cent of the triangles. After four steps, we obtain the triangulation shown in Figure 10(b). Note that the error indicator has successfully identified the corner singularity. In Figure 7 the norm of the error for global and adaptive refinement is compared. The slow convergence is due to the geometrical singularity. With the aid of the adaptive mesh refinement strategy, this problem is overcome. Also, note that most of the elements of the stiffness matrix after adaptive refinement can be retrieved from the earlier one.

## 5 Concluding remarks

In this paper, Powell-Sabin splines are used for the numerical solution of two-dimensional PDEs defined on irregular domains. A Powell-Sabin spline possesses many nice properties that make them very suitable for approximation of the PDE solution in finite element algorithms: they are  $C^1$ -continuous, and can be efficiently represented in a compact normalized B-spline basis. The Powell-Sabin B-splines can be chosen in a flexible way by means of PS-triangles. That allowed us to construct particular PS B-splines for treating the boundary conditions more easily. We

have elaborated a Galerkin-type PDE discretisation with an error of the order  $\mathcal{O}(h_{\max}^3)$  for the variable coefficient diffusion equation. In case of constant diffusion on each element an analytical formulation is given for the stiffness matrix elements. Finally, an a posteriori local error indicator was proposed, and integrated in an adaptive mesh refinement strategy. We strongly believe that it is worthwhile to further investigate the practical use of PS-splines for solving PDEs.

## References

- [1] C.K. Chui and M.J. Lai. Multivariate vertex splines and finite elements. *Journal of Approximation Theory*, 60:245–343, 1990.
- [2] P.G. Ciarlet. *The finite element method for elliptic problems*. Studies in mathematics and its applications. North-Holland publishing company, 1979.
- [3] C. de Boor. On calculating with B-splines. *Journal of Approximation Theory*, 6:50–62, 1972.
- [4] P. Dierckx. *Curve and Surface Fitting with Splines*. Oxford University Press, Oxford, 1993.
- [5] P. Dierckx. On calculating normalized Powell-Sabin B-splines. *Computer Aided Geometric Design*, 15:61–78, 1997.
- [6] P. Dierckx, S. Van Leemput, and T. Vermeire. Algorithms for surface fitting using Powell-Sabin splines. *IMA Journal of Numerical Analysis*, 12:271–299, 1992.
- [7] G. Farin. Triangular Bernstein-Bézier patches. *Computer Aided Geometric Design*, 3:83–127, 1986.
- [8] H. Melbø. A posteriori error estimation for finite element methods, an overview. Technical Report 6/01, Department of Mathematic Sciences, NTNU, Norway, 2001.
- [9] M.J.D. Powell and M.A. Sabin. Piecewise quadratic approximations on triangles. *ACM Transactions on Mathematical Software*, 3:316–325, 1977.
- [10] M.C. Rivara. Algorithms for refining triangular grids suitable for adaptive and multigrid techniques. *International Journal for Numerical Methods in Engineering*, 20:745–756, 1984.
- [11] X. Shi, S. Wang, and R.H. Wang. The  $C^1$ -quadratic spline space on triangulations. Technical Report 86004, Department of Mathematics, Jilin University, Changchun, 1986.
- [12] G. Strang and G.J. Fix. *An analysis of the finite element method*. Prentice-Hall, Englewood Cliffs, N.J., 1973.
- [13] E. Vanraes, P. Dierckx, and A. Bultheel. On the choice of the PS-triangles. Technical Report 353, Department of Computer Science, K.U. Leuven, 2003.
- [14] E. Vanraes, J. Maes, and A. Bultheel. Powell-Sabin spline wavelets. *International Journal of Wavelets, Multiresolution and Information Processing*, 2(1):23–42, 2004.
- [15] K. Willemans and P. Dierckx. Surface fitting using convex Powell-Sabin splines. *Journal of Computational and Applied Mathematics*, 56:263–282, 1994.
- [16] J. Windmolders. *Powell-Sabin splines for computer aided geometric design*. PhD thesis, Department of Computer Science, K.U. Leuven, 2003.
- [17] J. Windmolders, E. Vanraes, P. Dierckx, and A. Bultheel. Uniform Powell-Sabin spline wavelets. *Journal of Computational and Applied Mathematics*, 154(1):125–142, 2003.